Note on the time evolution sample for an adiabatic case

A. Initial condition and parameter settings

Here we consider the iso-curvature perturbation generated by a massless scalar field ϕ. We assume that the massless scalar field does not contribute to the background metric of the gradient expansion. Then, as is described in Ref. [1], once the spatial profile $\Upsilon(\boldsymbol{x})$ of the scalar field is specified at the leading order of the gradient expansion, the growing mode solution can be described up through the next-to-leading order of the long-wavelength approximation. We use the analytic expressions for the geometrical variables with the constant-mean-curvature and zero-shift gauge up through the next-to-leading order as the initial data for the sample code.

In this sample code, we consider the numerical domain given by $-L \leq X \leq L$, $0 \leq Y \leq L$ and $0 \leq Z \leq L$ with X, Y and Z being the reference Cartesian coordinates. The specific profile of Υ is the same as in Ref. [1]:

$$\Upsilon = \mu \exp\left(-\frac{1}{6}k^2R^2\right) W(R), \tag{1}$$

where $R = X^2 + Y^2 + Z^2$ and the function $W(R)$ is given by [2]

$$W(R; R_{\rm W}, L) = \begin{cases} 1 & \text{for } 0 \leq R \leq R_{\rm W} \\ 1 - \frac{\left((R_{\rm W}-L)^6 - (L-R)^6\right)^6}{(R_{\rm W}-L)^{36}} & \text{for } R_{\rm W} \leq R \leq L \\ 0 & \text{for } L \leq R \end{cases} \tag{2}$$

with $R_{\rm W} = 0.8L$. The parameters k and μ are set as $k = 10/L$ and $\mu = 0.64$. The amplitude μ is slightly larger than the threshold value $\mu_{\rm th} \simeq 0.63$ for PBH formation reported in Ref. [3].

The background universe is assumed to be radiation dominated, and the Hubble parameter at the initial time $H_{\rm i}$ is set to be $H_{\rm i} = 50/L$. The coordinate length L is covered by 40 grid points with grids on both ends. Since this sample code is just for demonstration, we do not seriously consider the constraint violations.

B. CARTOON method

The spherically symmetric numerical code COSMOS-s is firstly used in Ref. [1]. We perform the spherically symmetric relativistic simulation by using the CARTOON method [4]. That is, we solve the evolution equations on the Z-axis and create the necessary data around it based on the spherical symmetry with the 3rd order spline interpolation. A schematic figure for the CARTOON method is shown in Fig. 1.

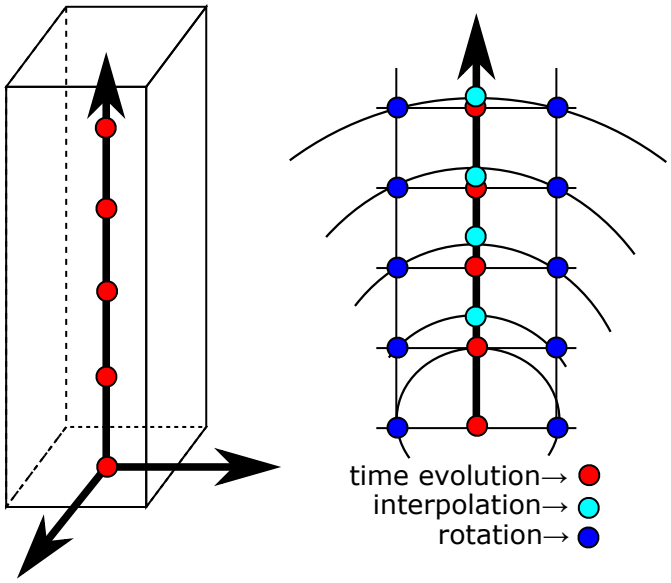

FIG. 1: A schematic figure for the CARTOON method.

C. Boundary condition

For the boundary condition, we adopt the asymptotically FLRW condition, but the constraints are significantly violated on the boundary through the time evolution. The constraint violation at the boundary starts to occur when the effects of the inhomogeneity reach the boundary, and the origin of the constraint violation is due to unphysical reflected modes. As far as we know, for the asymptotically FLRW boundary, no established procedure to reduce the unphysical reflected modes has been reported. Therefore the time evolution should be terminated before the boundary effects influence the dynamics of interest. We do not seriously check this issue in this sample code. Because it is just for a demonstration. In order to avoid detect the significant constraint violation due to the boundary effect, we exclude the outer 1/20 region from the region for checking the constraint violation. The user who wants to change the region has to change the value of the parameter exclude_boundary_rate in `cosmos_s.h`.

D. Non-Cartesian coordinate

In this sample code, we employ the non-Cartesian coordinate system (x, y, z) firstly implemented in Ref. [2]. The non-Cartesian coordinate z is related to the Cartesian coordinate Z as follows:

$$Z = z - \frac{\eta}{1+\eta}\frac{L}{\pi}\sin\left(\frac{\pi}{L}z\right). \tag{3}$$

This functional form satisfies $z = 0$ at $Z = 0$ and $z = L$ at $Z = L$. At the origin, the infinitesimal interval in the Cartesian coordinate ΔZ is covered by the non-Cartesian

coordinate interval $\Delta z = (1+\eta)\Delta Z$. Therefore the central part is enlarged in this non-Cartesian coordinates.

E. Mesh refinement

On top of the non-Cartesian coordinate system, we implement fixed mesh refinement. We do not explain the details of our mesh refinement procedure, but the values on 9 outer gird points in a higher layer are calculated from the interpolation with the values in the lower layer. The given values on the 9 grid points are discarded when the lower layer data is updated. In the sample code, 3 additional layers of for the mesh refinement are introduced when the value of the lapse function at the origin reduces to 0.1 0.075 and 0.05. The region covered by one higher layer is the region covered by 100 grids in the lower layer. These parameters for the mesh refinement can be controlled by the parameter file `par_fmr.d`.

F. Excision

After the black hole formation, we excise a central region inside the horizon. The number of excised grid points is controlled by the parameter *excision grid number* in the parameter file `par_ini.d`. On these gird points, we extrapolate each function with a quadratic form by using the data just outside the excised region. If the numerical simulation crashes due to the instability associated with the excision procedure, the procedure itself or the excised region should be changed. But, as long as the numerical simulation does not crash and the behavior inside the horizon does not affect the outside horizon, we need not care about it if we are only interested in the outside region.

G. Results of the time evolution

In the default setting, the time evolution starts from the initial data described above. Then one find PBH formation at around the coordinate time $t \simeq 18.9L$. It takes some time. We also attached the data file `ini_all.dat` which describes the system soon after the horizon formation. For instance, one can set the value of "*maximum step of the main loop*" in `par_ini.d` to 1 and set the value of the line indicated by "*0:no continue 1:continue*" to 1. When the numerical code is executed, first the data file `ini_all.dat`, in which 3 higher layers are already introduced, is loaded. After just one step of the evolution, all the data will be recorded into `out_all.dat`, and the calculation stops. The value of the lapse function on the x-axis at $t = 18.9L$ is depicted as a function of x in Fig. 2. The result with the sample 3+1 code in the same setting is also shown for reference. The value of the scalar field ϕ is depicted in Fig. 3. The result with the sample 3+1 code in the same setting is also shown

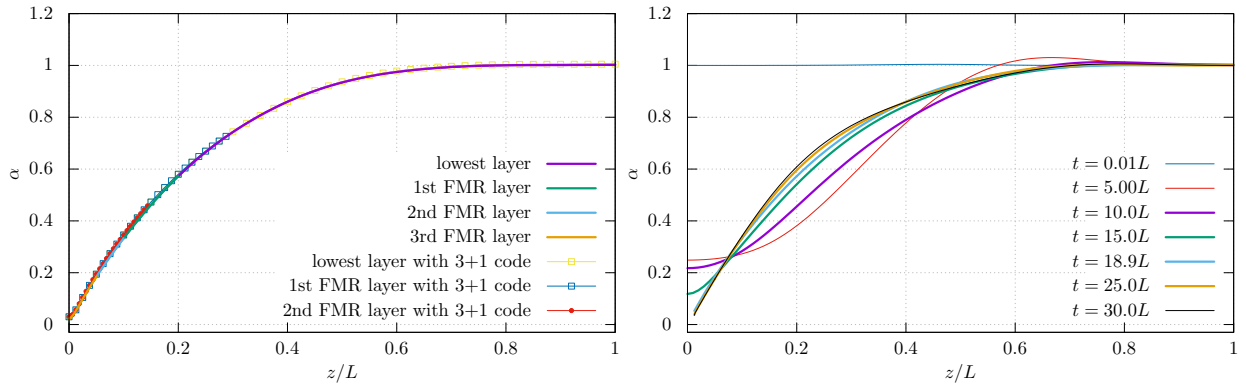

FIG. 2: The lapse function generated from 1s and 2nd columns in `out_jkz.dat` at the horizon formation (left) and snapshots of the lapse function with the excision procedure (right). In the right figure, the data are not plotted in the excised region after the horizon formation.

for reference. [1]

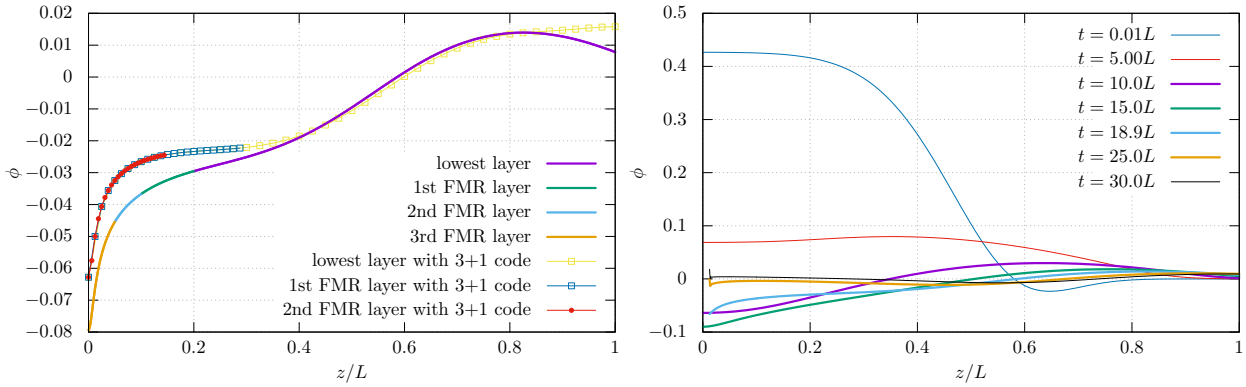

FIG. 3: The scalar field ϕ generated from 1st and 47th columns in `out_jkz.dat` at the horizon formation (left) and snapshots of the scalar field with the excision procedure (right). In the right figure, the data are not plotted in the excised region after the horizon formation.

H. Horizons

The trajectories of future and past trapping horizons are shown in Fig. 4. The horizon trajectories for each mesh refinenment layer are recorded in the file `out_horizon_xx.dat` if they are found, where "xx" is the number of the layer. The first column is the recorded

[1] The behavior of the scalar field is different from that given in the 3+1 dimensional sample code in ths same setting. This would be because of the low resolution in the 3+1 dimensional sample code and difference of the outer boundary condition.

time and the coordinate radius and the areal radius are recorded in the $2n$-th and $(2n+1)$-th columns with $n = 1, 2, \cdots$, respectively. When excision procedure becomes active, the region inside the initial radius of the future trapping horizon is excluded from the explored region.

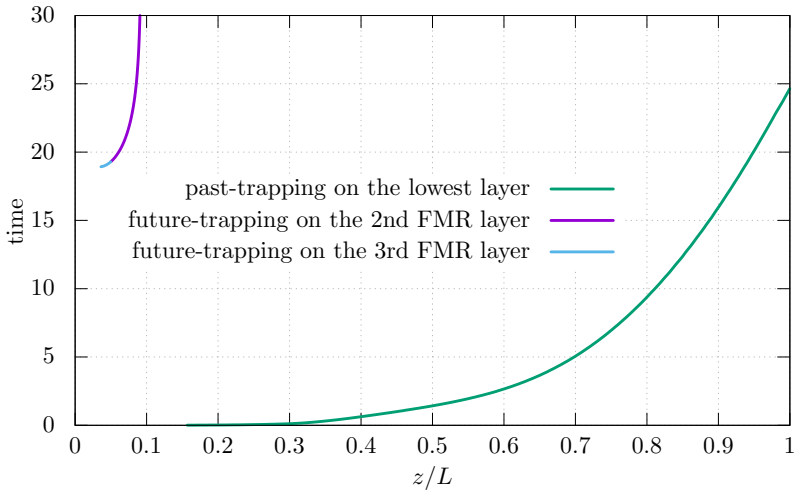

FIG. 4: Future and past trapping horizon trajectories.

[1] C.-M. Yoo, T. Harada, S. Hirano, H. Okawa, and M. Sasaki, Phys. Rev. D **105**, 103538 (2022), arXiv:2112.12335, *Primordial black hole formation from massless scalar isocurvature.*

[2] C.-M. Yoo, T. Ikeda, and H. Okawa, Class. Quant. Grav. **36**, 075004 (2019), arXiv:1811.00762, *Gravitational Collapse of a Massless Scalar Field in a Periodic Box.*

[3] C.-M. Yoo, T. Harada, and H. Okawa, Phys. Rev. D **102**, 043526 (2020), arXiv:2004.01042, *Threshold of Primordial Black Hole Formation in Nonspherical Collapse*, [Erratum: Phys.Rev.D 107, 049901 (2023)].

[4] M. Alcubierre *et al.*, Int. J. Mod. Phys. D **10**, 273 (2001), arXiv:gr-qc/9908012, *Symmetry without symmetry: Numerical simulation of axisymmetric systems using Cartesian grids.*